A microscopic view of substitution reactions solvated by ionic liquids

Guilherme M. Arantes[a] and Mauro C. C. Ribeiro
Laboratório de Espectroscopia Molecular, Instituto de Química, Universidade de São Paulo, C.P. 26077, CEP 05513-970 São Paulo, Brazil

(Received 11 January 2008; accepted 7 February 2008; published online 18 March 2008)

The solvation effect of the ionic liquid 1-*N*-butyl-3-methylimidazolium hexafluorophosphate on nucleophilic substitution reactions of halides toward the aliphatic carbon of methyl *p*-nitrobenzenesulfonate (*p*NBS) was investigated by computer simulations. The calculations were performed by using a hybrid quantum-mechanical/molecular-mechanical (QM/MM) methodology. A semiempirical Hamiltonian was first parametrized on the basis of comparison with *ab initio* calculations for Cl^- and Br^- reaction with *p*NBS at gas phase. In condensed phase, free energy profiles were obtained for both reactions. The calculated reaction barriers are in agreement with experiment. The structure of species solvated by the ionic liquid was followed along the reaction progress from the reagents, through the transition state, to the final products. The simulations indicate that this substitution reaction in the ionic liquid is slower than in nonpolar molecular solvents proper to significant stabilization of the halide anion by the ionic liquid in comparison with the transition state with delocalized charge. Solute-solvent interactions in the first solvation shell contain several hydrogen bonds that are formed or broken in response to charge density variation along the reaction coordinate. The detailed structural analysis can be used to rationalize the design of new ionic liquids with tailored solvation properties. © *2008 American Institute of Physics*. [DOI: 10.1063/1.2890042]

I. INTRODUCTION

Ionic systems with low melting temperature, say, below 100 °C, previously called as room temperature molten salt, are now simply called ionic liquids (ILs). In the last decade, ILs have emerged as promising solvents for environmentally friendly organic synthesis, electrodeposition, and electrolytes for electrochemical devices. In fact, the most common application of ILs is their use as alternative solvents in industrial applications. Despite this technological interest, a detailed microscopic view of the role played by the structure and the dynamics of ILs as reaction media is still lacking.[1–3]

Ionic liquids usually contain large organic ions that reduce the strong ionic interactions with a concomitant decrease of melting temperature. Among many ILs that have been synthesized, common systems are based on aromatic ammonium salts, such as pyridinium or imidazolium cations. The anions can be simple inorganic species (BF_4^-, PF_6^-, etc.) or more complex species such as $[(CF_3SO_2)_2N]^-$, bis(trifluoromethanesulfonyl)imide. In this work, we are concerned with a well-known IL, namely, 1-*N*-butyl-3-methylimidazolium hexafluorophosphate, $[BMIM]PF_6$ (Fig. 1).

Probably, the best characterized reaction solvated by ILs is the halide nucleophilic substitution toward the aliphatic carbon of methyl *p*-nitrobenzenesulfonate (Fig. 2).[4–7] Reaction rates and activation parameters in a variety of ILs were measured for this process, for which the reaction rate in IL is generally slower than in dichloromethane. This is in line with the Hughes–Ingold interpretation that the more polar solvent stabilizes the halide ion and increases the reaction barrier.[8,9] However, this interpretation seems to fail when applied to the differences observed between ILs.[6] Lancaster and collaborators have used empirical spectroscopic parameters, such as the Kamlet–Taft parameters,[10] to assign a polarity index to ILs.[5,7] This approach is not free from pitfalls[11] and also do not explain satisfactorily all of the observed differences on rates and activation parameters. Actually, the very own concept of polarity of ILs has been recently criticized.[3] Hence, a microscopic understanding of the IL solvation structure in the halide substitution toward *p*-nitrobenzenesulfonate would shed light on this well characterized process and also on the class of nucleophilic substitution reactions solvated by ILs.

Computer simulation has become a fundamental tool for revealing the microscopic structure and dynamics of ILs. Several simulation studies analyzed pure ILs (Refs. 12–15) and solutions of small[16–18] and large[19,20] molecules in ILs. However, to our knowledge, only one computational study, by Acevedo *et al.*,[21] investigated a chemical reaction. These authors simulated a Diels–Alder condensation in acidic and basic mixtures of 1-ethyl-3-methylimidazolium chloride and chloroaluminate ($AlCl_3$).

In this work, we performed the first computer simulations of a nucleophilic substitution reaction solvated by a pure IL. A hybrid quantum-mechanical/molecular-mechanical (QM/MM) potential was used in order to provide an explicit representation of the reactant solutes and the solvent.[22–24] A QM semiempirical Hamiltonian was first calibrated specifically to the halide substitution reaction at gas phase, whereas the MM force field for $[BMIM]PF_6$ was taken from previous simulations of the pure IL. Free energy profiles of the nucleophilic substitution reaction taken place

[a]Electronic mail: garantes@iq.usp.br.

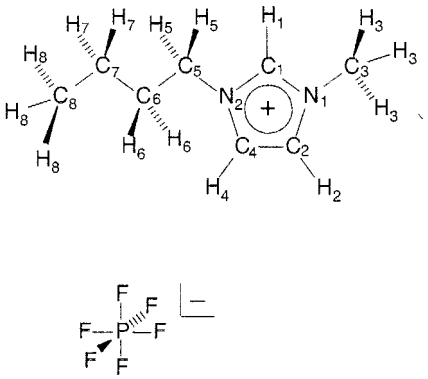

FIG. 1. Structure and atom numbering for 1-butyl-3-methyl-imidazolium [BMIM] and PF_6^-.

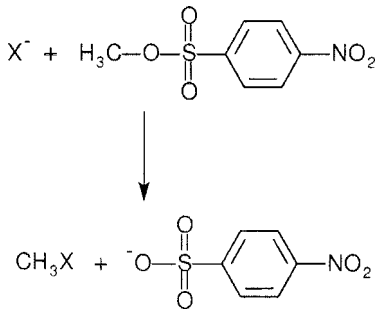

FIG. 2. Halide nucleophilic substitution of methyl *p*-nitrobenzenesulfonate. $X^-=Cl^-$ or Br^-.

in the IL environment were then evaluated. Proper to the microscopic detail provided by the QM/MM methodology, we followed the solvation structure around solutes from the reagents to the reaction products through the transition state. The computer simulations indicate that the classical Hughes–Ingold interpretation for reactions in molecular solvents also holds for the reactions studied in this work.

II. METHODS

A. Electronic structure calculations

Pathways for the substitution reactions (Fig. 2) isolated in the gas phase were obtained by calculations with the GAUSSIAN-98 program.[25] Reactant, transition state (TS), and product geometries were fully optimized by the analytic gradient method, using the density functional B3LYP (Refs. 26 and 27) and 6-31+G(d,p) basis set.[28] Vibrational frequencies were calculated in the same theory level. No imaginary frequency was found for minima and only one was found for TSs.[29] Energy of the stationary points was recalculated with the MP2 level in the frozen-core approximation[30] with the 6-311+G$(2df,2p)$ basis set,[31] and also with the semiempirical Hamiltonians AM1,[32] PM3,[33] and the specifically calibrated set obtained here (see next section). The latter was employed to describe the QM region in the hybrid QM/MM simulations.

B. Parametrization of the semiempirical Hamiltonian

The approach proposed by Rossi and Truhlar,[34] later applied by Arantes and Loos,[35] was used. In this approach, *ab initio* properties calculated in the gas phase are used as references in the training or data set for the specific parametrization.

The calibration precedure has already been described in detail.[35] Here, the parameters for the NDDO Hamiltonian were optimized by minimizing the error function,

$$P=\sum_{m}^{M} W_m \frac{[\Delta E_m^{\mathrm{NDDO}}-\Delta E_m^{\mathrm{AI}}]^2}{[\Delta E_m^{\mathrm{AI}}]^2}, \tag{1}$$

where $\Delta E_m^{\mathrm{NDDO}}$ and ΔE_m^{AI} are the electronic and nuclear repulsion contributions to the relative energy calculated in the NDDO semiempirical and *ab initio* levels, respectively. W_m is the weight given and there is a total of M molecules in the training set. A combination of genetic algorithm and simplex is used for P minimization.[36,35]

The training set contained reactants, TSs, and products for the substitution reactions shown in Fig. 2 and Table II. Additionally, the following species were included:

(1) four geometries along the reaction pathway with the forming bond (C–X, where X=Cl or Br) constrained and other four geometries with the breaking bond (C–O) constrained;
(2) three geometries of phenyl sulfonate with different torsions of the S–C bond;
(3) four geometries of *p*NBS with C–O and O–S bonds broken and reformed, obtained with the original PM3 method[33] but unstable when described by *ab initio* methods;
(4) four geometries along the pathway for hydrogen abstraction from the methyl group in *p*NBS by Cl^- and Br^- each; and
(5) three geometries along the pathway for hydrogen abstraction from the methyl group in CH_3Br by phenyl sulfonate oxygen.

Energies and geometries were obtained as described in the previous section. Species listed in items (2) and (3) were included because geometries optimized with the original PM3 Hamiltonian were unstable. Species listed in items (4) and (5) were included to calibrate the affinity of the nucleophiles and leaving group for the alkyl proton. Weights used during the minimization of Eq. (1) were $W_m=5$ to the stationary points and to the species listed in item (1) above; $W_m=1$ for species listed in items (2)–(5).

Original PM3 parameters were used as starting points. Parameters U_{ss}, U_{pp}, β_s, β_p, α, K_i, L_i, and M_i, where $i=1$ and 2, were optimized to elements S, Cl, and Br. These elements were chosen because they are directly involved in the formation of bonds or because high deviations are observed for properties obtained with the original parametrization for molecules containing such elements.[33] The remaining parameters for S, Cl, and Br and the parameters for the other elements were not changed from the original PM3 values. A variation of ±20% from the original values was allowed for U, β, and α, and $-0.30<K_i<0.30$ eV Å, $0.0<L_i<8.0$ Å^{-2}, and $0.0<M_i<3.0$ Å. Semiempirical computations for iso-

TABLE I. Specific reaction semiempirical parameters obtained for S, Cl, and Br. Parameters that are not shown are the same as the original PM3 set.

		RECAL		
Parameters	Units	S	Cl	Br
U_{ss}	eV	−40.726 94	−102.690 54	−135.851 82
U_{pp}	eV	−49.562 35	−53.348 77	−74.090 39
β_s	eV	−7.469 77	−26.578 86	−31.205 94
β_p	eV	−8.319 44	−10.720 06	−6.684 30
α	Å^{-1}	2.712 740	2.808 928	2.3745 36
K_1	eV Å	0.165 011	0.280 346	0.0463 64
K_2	eV Å	0.035 709	0.160 979	−0.0243 34
L_1	Å^{-2}	4.990 531	4.750 555	2.7504 36
L_2	Å^{-2}	6.468 346	5.076 629	3.9019 98
M_1	Å	2.173 107	1.311 406	0.1332 15
M_2	Å	1.624 377	0.751 976	1.8912 73

lated species in the gas phase were carried with the GEOMOP program.[37]

The parameters obtained are shown in Table I and the performance of the calibrated Hamiltonian can be evaluated through Table II. In comparison with the *ab initio* reference, the error in TS and reaction energies is smaller than 2 kJ/mol.

C. Potential energy function

The MM energy function used to describe $[BMIM]PF_6$ is based on the OPLS-AA (Ref. 38) force field. For $[BMIM]^+$, covalent and Lennard–Jones parameters were taken from Margulis *et al.*[12] and atomic charges from de Andrade *et al.*[14] The atomic charges given by de Andrade *et al.* result in a dipole moment at the $[BMIM]^+$ center of mass $\mu=4.27$ D, which is in good agreement with the calculated *ab initio* $\mu=4.32$ D. On the other hand, atomic charges given by Margulis *et al.* result in $\mu=1.74$ D.[15] Atomic charges and Lennard–Jones parameters for PF_6^- were taken from Margulis *et al.*, but covalent parameters for this anion were not given in their original reference,[12] so that we used the ones reported by Morrow and Maginn.[13] It should be noted that unities given in the original report were erroneous.[39] The classical potential used to describe the *p*NBS solute is also based on the OPLS-AA (Refs. 38 and 40) force field, with some missing parameters taken from the general AMBER force field.[41] Tables with the parameters used are available from the authors upon request.

D. Free energy profile

Initial configurations used for the calculation of free energy profiles contained one *p*NBS molecule and one nucleophile (Cl^- or Br^-, see Fig. 2), solvated by 198 $[BMIM]^+$ and 197 PF_6^- ions, as described in Sec. II E. A hybrid QM/MM potential was used to compute the reaction free energy profiles. Reactants were described in the QM region by the calibrated semiempirical Hamiltonian, and the IL solvent was described in the MM region. Hence, there was no covalent bond in the boundary of the QM and the MM regions. Interactions between the two regions occur via polarization of the QM region by the atomic partial charges in the MM region and via van der Waals interactions described by a Lennard–Jones potential between QM and MM atoms.[22,23] Lennard–Jones parameters for the QM atoms were the same as used for the MM simulations. This approach has been successfully used in many studies of chemical reactivity in condensed phase.[24]

The free energy profile is the potential of mean force calculated along a reaction coordinate ξ. The reaction coordinate was defined as the difference between the broken and the formed bonds to methyl carbon, $\xi=d(CO)-d(XC)$ (X $=Cl^-$ or Br^-, see Fig. 2). Sampling along the reaction coordinate was enhanced with a harmonic umbrella potential.[42] Reference reaction coordinates ξ_i were equally spaced at 0.10 Å and a constant $k_{umb}=1000$ kJ mol^{-1} Å^{-2} was used. Molecular dynamics using the velocity Verlet–Langevin algorithm[43] with a friction coefficient $\gamma=25$ ps^{-1} were run for 60 ps of equilibration and 100 ps of data collection for each reference window. A total of 36 simulation windows covered the reaction coordinate from reactants to products. Potentials of mean force were finally calculated by the weighted histogram analysis method[42] (WHAM) from the ξ occurrence collected at each time step during the molecular dynamics. This procedure has been described in more detail before.[44]

E. Simulation details

An initial configuration containing 200 $[BMIM]PF_6$ was built from a previous configuration[15] in which a united-atom model was used. The missing hydrogens and fluorines were added by using the heavy atom and the phosphorus coordinates, respectively, and the equilibrium bond length with the missing atom. This initial configuration was optimized by the conjugated gradient method[45] with the position of all atoms frozen, except hydrogen and fluorine.

TABLE II. Relative energy (in kJ/mol) calculated by different electronic structure methods for the TS and products formed in the halide substitution reaction of *p*NBS in the gas phase (Fig. 2). AM1 and PM3 are original semiempirical parametrizations (Refs. 32 and 33), RECAL is the recalibrated semiempirical set obtained in this study, and *ab initio* is MP2/6-311+G(2*df*,2*p*)//B3LYP/6-31+G(*d*,*p*).

Halide		AM1	PM3	RECAL	*Ab initio*
Br^-	ΔE_{TS}	···	21.3	−20.8	−19.5
	ΔE_{prod}	−191.6	−22.0	−88.6	−86.6
Cl^-	ΔE_{TS}	−16.2	27.3	−40.8	−42.0
	ΔE_{prod}	−129.9	−68.9	−125.0	−126.3

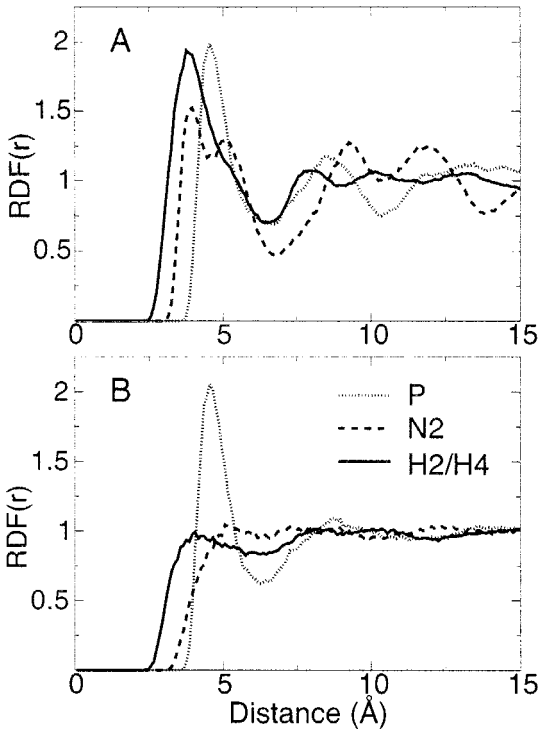

FIG. 3. Radial distribution functions between the methyl carbon of *p*NBS (C0) and $[BMIM]PF_6$ centers shown in legend. Upper panel (A) was obtained at 300 K and lower panel (B) was obtained at 450 K. See Fig. 1 for [BMIM] atom numbering.

A 10 ps molecular dynamics run was carried out from this optimized configuration. Harmonic constraints were used to tether the heavy atoms to their initial positions. The force constant used was gradually reduced from 1000 kJ mol^{-1} $Å^{-2}$ to 0, and the temperature was gradually increased to 300 K. This box was equilibrated for 500 ps and a trajectory of 2 ns was recorded (with each stored frame spaced in 50 fs). The side of the periodic cubic box was 41.842 Å, giving a density $\rho=1.29$ g/cm^3, which is close to the experimental density at 303 K, $\rho=1.37$ g/cm^3.[15] The average electrostatic potential energy was −177 kJ/mol, and the average Lennard–Jones interaction was −57 kJ/mol. The root-mean-squared deviations from the mean values of the temperature was 2 K and 0.7% of the total potential energy. These results and radial distribution functions obtained for the pure IL (data not shown) agree with previous simulations of pure $[BMIM]PF_6$.[15,14,13]

A configuration of *p*NBS solvated by $[BMIM]PF_6$ was obtained by superimposing one molecule of *p*NBS to the center of the previously equilibrated $[BMIM]PF_6$ box. IL species that were less than 3.0 Å apart from *p*NBS were removed, resulting in a box with one *p*NBS and 198 $[BMIM]PF_6$. The system was relaxed again for 10 ps molecular dynamics with decreasing harmonic constraints and equilibrated for 200 ps at 300 K. A configuration at 450 K was generated by increasing the temperature in three steps of 50 K for 150 ps of molecular dynamics and further equilibrated for 200 ps at 450 K. Trajectories of 2 ns were recorded at 300 and 450 K for analysis of the *p*NBS solvation by $[BMIM]PF_6$. The first coordination sphere of PF_6^- anions around the methyl group of *p*NBS contained on average three anions. Each of these was mutated to Cl^- or Br^- to generate three different starting structures at each temperature for the calculation of reaction free energy profiles.

Classical molecular dynamics simulations with pure MM potentials were executed in the *NPT* ensemble. Equations of motion were integrated with a leapfrog-Verlet algorithm. The Berendsen temperature and pressure controls were used with a coupling constant of 0.1 ps for the thermostat. For the barostat, a value of 2.10^3 ps atm was used for the ratio (τ_P/β_T) between the coupling constant and the isothermal compressibility.[45] All the simulations reported used a time step of 1 fs. Periodic boundary conditions were considered in all molecular dynamics runs. An atom-based force-switching truncation scheme was used in the nonbonding interactions with $r_{on}=8$ Å and $r_{off}=12$ Å for both pure MM and QM/MM interactions[23] when using a hybrid potential. Tests performed in other systems indicated that results obtained within this scheme are equivalent to results obtained without truncation.[46,44] All simulations and free energy calculations were performed with the DYNAMO library.[23]

III. RESULTS AND DISCUSSION

A. Parametrization of the semiempirical Hamiltonian

Stationary points for the substitution reactions in the gas phase were calculated by *ab initio* methods as reference values to compare with approximate semiempirical Hamiltonians, so that the best semiempirical method could be chosen and used to generate free energy profiles in condensed phase. It was soon realized that standard semiempirical Hamiltonians, such as AM1 and PM3, were not reliable for the description of the electronic structure of halogen substitution reactions. Table II shows energies for product and TS formations relative to the reagent energy calculated by several methods. Both AM1 and PM3 Hamiltonians show deviations from the *ab initio* reference as large as 100 kJ/mol. We resorted to a reparametrization of the semiempirical Hamiltonian specifically to the reactions of interest (Fig. 2). In particular, parameters for S, Cl, and Br were calibrated to reproduce *ab initio* data.[34,35] The performance of the reparametrized set is excellent, and deviations from the *ab initio* reference are not larger than 2 kJ/mol. It should be noted that a negative relative energy for TS formation does not mean that the activation energy for the reaction is negative. Activation energy should be measured from ion-molecule complexes which are formed between reagents in the gas phase and are more stable than the separated reagents. Ion-molecule complexes were not obtained here because this work is not concerned with the gas phase reaction.

The reparametrized set can be used to calculate energies of reaction species with precision similar to MP2/6-311 $+G(2df,2p)$, which was the theory level used to generate the parametrization training set. However, whereas the MP2 theory is prohibitively slow for the calculation of free energy profiles, the semiempirical methodology is much less demanding on computational time.

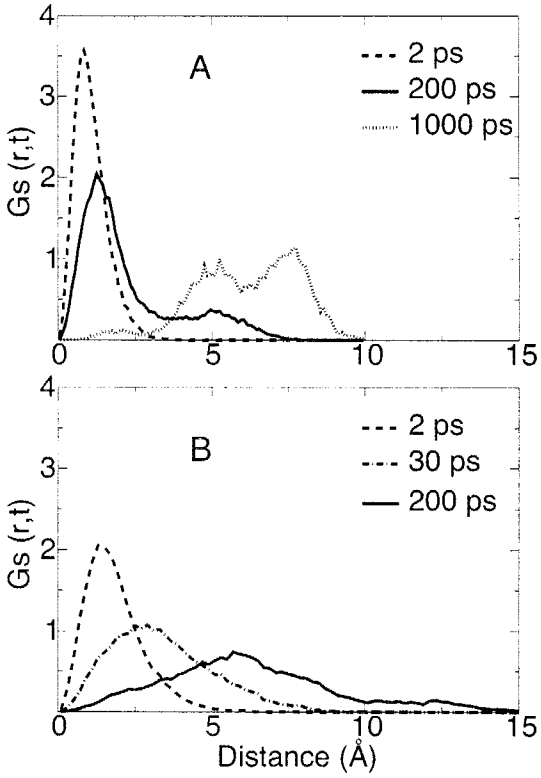

FIG. 4. Self-part of the van Hove correlation function calculated at indicated times for the *p*NBS methyl carbon (C0) site solvated by $[BMIM]PF_6$. Upper panel (A) was obtained at 300 K and lower panel (B) was obtained at 450 K.

B. Structure and dynamics of IL solvating *p*NBS

This section discusses the equilibrium structure and dynamics of IL species solvating *p*NBS, in particular, its methyl carbon (C0), obtained by classic MM simulations. Visual inspection of snapshots of arbitrary configurations obtained from the molecular dynamics simulations (see Fig. 7) suggests that *p*NBS occupies a position similar to a $[BMIM]^+$ cation in pure $[BMIM]PF_6$. This is expected since isolated *p*NBS and $[BMIM]^+$ have similar structures (both have a rigid aromatic ring and a flexible chain), and *p*NBS has a dipole moment $\mu=3.9$ D close to $[BMIM]^+$, $\mu=4.32$ D.[15]

Figure 3 shows partial radial distribution functions (RDFs) between the solute *p*NBS methyl carbon (C0) and anions and cations of the IL. At 300 K, the RDFs have a well-defined structure, with clear first and second peaks, indicating that there are distinguishable solvation shells around the *p*NBS methyl carbon. These solvation shells are more defined for the C0–P RDF than they are for the C0–N2 (N2 is the atom in $[BMIM]^+$ closest to its center of mass), so that the cation distribution in the second solvation shell around *p*NBS methyl carbon is rather disordered. A coordination number $N=3$ is obtained by integrating the C0–P RDF up to the first minimum (7 Å), indicating that there are three anions around the *p*NBS methyl carbon. At 450 K, however, there is essentially no structure in the C0–N2 and C0–H2/H4 RDFs besides the excluded volume. Hence, the cation distribution around the *p*NBS methyl carbon is almost random. On the other hand, the first coordination shell of anions around the *p*NBS methyl carbon is still well-defined with coordination number of 3 anions, even in the more mobile IL at 450 K.

The IL solvation dynamics was analyzed by the calculation of the van Hove correlation function.[43] For the pure $[BMIM]PF_6$ (results not shown here), the calculated functions agree with previous simulations,[47,13] indicating that the force field used here is also appropriate to describe the structural relaxation. Figure 4 shows the self-part of the van Hove correlation function $[G_s(r,t)]$ calculated for the *p*NBS methyl carbon. At 300 K, the solute mobility, in particular, the *p*NBS methyl carbon, is rather small. After 1 ns, this site moves on average only ~6 Å from its original location. It is clear from $[G_s(r,t)]$ at 300 K and $t=200$ ps that there is a division of populations for the C0 site. This is partially due to the *p*NBS methyl group flexibility, in particular, the S–OC bond torsion, but more importantly, this is due to hopping through different configuration domains, which is characteristic of solvation in glass-forming liquids.[48] No population separation is observed at 450 K, partially because the S–OC bond torsion should be observed more often, but mostly because the *p*NBS methyl group has a diffusive behavior, which is characteristic of solvation in normal liquids.[48] It is worth mentioning that translational motion of the solute is higher than the $[BMIM]^+$ motion either at 300 or 450 K (data not shown). Thus, even though both the *p*NBS and the $[BMIM]^+$ species have similar structures, charge neutrality of *p*NBS allows a higher mobility because there is no ionic pair such as the one between $[BMIM]^+$ and PF_6^-.

The coordination of PF_6^- anions around *p*NBS methyl carbon is the main feature in the static distribution functions

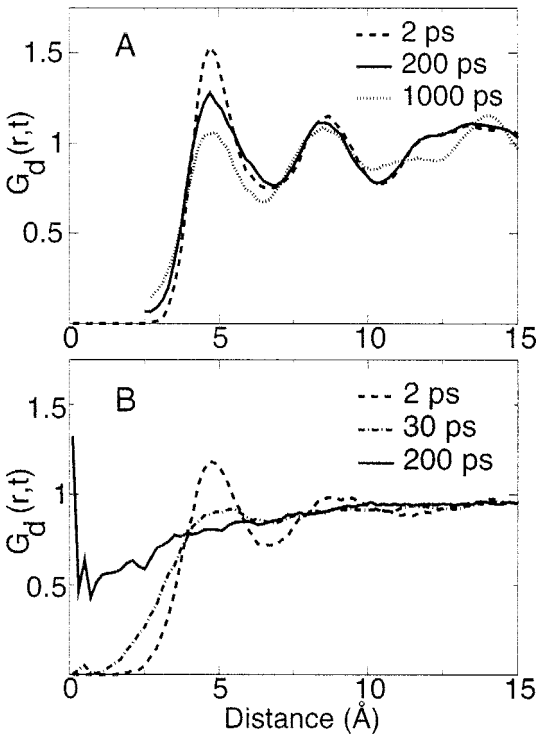

FIG. 5. Distinct part of the van Hove correlation function calculated at indicated times between *p*NBS methyl carbon (C0) and PF_6^- phosphorus. Upper panel (A) was obtained at 300 K and lower panel (B) was obtained at 450 K.

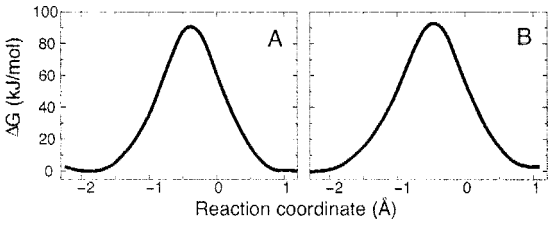

FIG. 6. Free energy profiles for reactions of Cl^- (left panel, A) and Br^- (right panel, B) with the *p*NBS methyl carbon solvated by $[BMIM]PF_6$ at 450 K. See text for the definition of reaction coordinate.

shown in Fig. 3. Figure 5 shows the distinct part of the van Hove correlation function $[G_d(r,t)]$ between these same sites. The solvation structure remains even after 1 ns at 300 K, indicating that the IL solvent is very rigid and immobile at this temperature. In fact, during the calculation of free energy profiles, we observed an unusually large variation (~30 kJ/mol) between profiles obtained from different starting structures for Cl^- reaction at 300 K. This variation decreased if the equilibration and data accumulation times during the molecular dynamics simulations increased, but it still remained as high as 15 kJ/mol with 60 ps for equilibration and 150 ps for data collection in each window.

On the other hand, Fig. 5 shows that the anion solvation around the *p*NBS methyl carbon is practically randomized at 450 K after 30 ps, when only a volume exclusion "memory" remains. As the IL mobility at this temperature is much higher, Fig. 5 suggests that 30 ps of equilibration and data accumulation would be enough to randomize the solvent structure around the *p*NBS methyl carbon. It was found that variations in free energy profiles calculated from different starting structures at 450 K were smaller to 10 kJ/mol with 30 ps of data accumulation. The variation was further reduced to less than 5 kJ/mol by using 60 ps of equilibration plus 100 ps of data accumulation in each window. The profiles shown in the following section were obtained with these simulation times.

C. Free energy profiles for substitution reactions

Figure 6 shows free energy profiles obtained for Cl^- and Br^- nucleophilic substitutions toward the *p*NBS methyl carbon solvated by $[BMIM]PF_6$ at 450 K. The free energies of activation are 91 ± 2 and 93 ± 2 kJ/mol for the Cl^- and the Br^- reactions, respectively. The error is the standard deviation from three profiles obtained with different starting structures (see Sec. II). This is a lower bound on the true simulation error. It is difficult to obtain a better estimate of this deviation because several factors contribute, such as sampling statistics and the potential energy function. A more realistic error value should be around 3 kcal/mol (or 12 kJ/mol).[35]

Lancaster and Welton determined experimental activation parameters by using the Eyring equation for the same reactions in $[BMIM]PF_6$.[6] These measurements suggest that the free energy of activation at 450 K should be within the range of 82–95 kJ/mol for the Cl^- reaction, in reasonable agreement with the present calculations. The calculated barrier for Br^- reaction is 2 kJ/mol higher than the barrier for

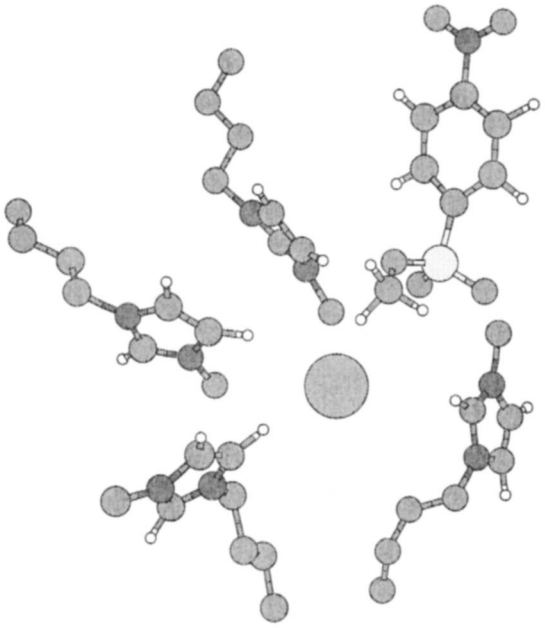

FIG. 7. Snapshot of a reagent configuration for the chloride substitution reaction at the methyl *p*NBS carbon solvated by $[BMIM]PF_6$. Parts of the IL were erased to ease visualization.

Cl^- reaction. This is also in agreement with the rate constants obtained by Lancaster and Welton, since the rate for Br^- reaction is approximately half the rate for Cl^- reaction at 298 K.[6] Although the experimental studies of Lancaster *et al.*[4,6] were carried out in concentrations and temperatures different from the simulated ones, the agreement between measured and calculated activation barriers suggests that the simulated model is realistic.

In the gas phase, the reactivity of chloride and bromide toward the *p*NBS methyl carbon differs considerably (Table II). Bromide reaction has a TS potential energy of about 20 kJ/mol higher, and a reaction potential energy of 40 kJ/mol higher, than chloride reaction. These differences are completely nullified when the reactions are solvated by the IL (Fig. 6). This "levelling effect," as called by Lancaster *et al.*, is observed on the rate constants measured for nucleophilic substitution reactions in several ILs.[7,6,5,4] The intrinsic differences in reactivity observed for the reactions in gas phase are compensated in ILs by differential solvation of reagent and TS species.

TABLE III. Calculated mean distances for the reaction of *p*NBS solvated in $[BMIM]PF_6$ (distances and standard deviations in Å). Values were calculated by analysis of the trajectories accumulated during 200 ps. Distances were evaluated in intervals of 50 fs (i.e., 4000 distance values were accumulated).

Centers	Reagent	TS	Products
	Reaction with Cl^-		
Cl–C0	3.34 ± 0.07	2.22 ± 0.07	1.98 ± 0.04
OC–C0	1.44 ± 0.04	1.87 ± 0.09	2.98 ± 0.07
	Reaction with Br^-		
Br–C0	3.55 ± 0.07	2.31 ± 0.06	2.04 ± 0.05
OC–C0	1.44 ± 0.04	1.83 ± 0.08	3.04 ± 0.08

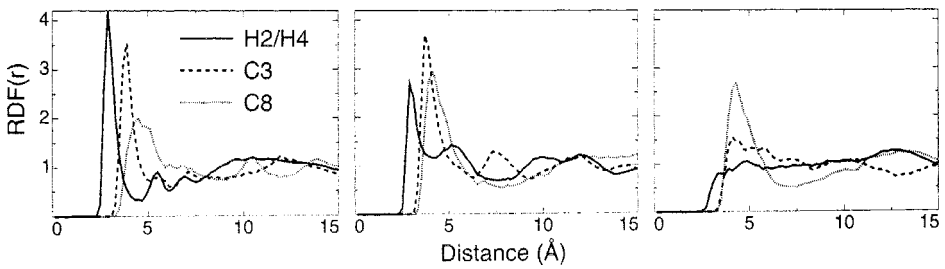

FIG. 8. Radial distribution functions at 450 K between the solute Cl^- and different IL centers shown in the legend. See Fig. 1 for [BMIM] atom numbering. Left panel was obtained for the reagent region, middle panel for the TS region, and right panel for the product region.

D. Structure of the IL solvating the reaction species

A snapshot of an arbitrary configuration taken from the molecular dynamics simulations in the reagent (ξ=−1.9 Å) region for the Cl^- reaction is shown in Fig. 7. Distances of forming and breaking bonds are shown in Table III for both halide reactions. The solvated TS structure is a pentacoordinate trigonal bipyramid with the nucleophile and the leaving group oxygen in opposite axial positions. This is similar to the gas phase structure (not shown) and usual S_N2 reactions at aliphatic carbon.[49] As expected, the Br–C0 distance is larger than the Cl–C0 distance in all reaction species. For the reagents, this difference is 0.2 Å, decreasing to 0.1 Å in the TS, and ~0.06 Å in the products (Table III). The distance between the leaving group oxygen (OC) and C0 is almost the same for all species in both reactions. The reaction mechanism is a typical bimolecular nucleophilic substitution, which is also called A_nD_n in the current IUPAC nomenclature.[50]

Analysis of the solvation structure around the reaction species was based on solute-solvent RDFs obtained from molecular dynamics trajectories accumulated for 200 ps in the reagent, TS, and product regions of the free energy profiles. The system was restricted to each region via an umbrella potential as described in Sec. II. The reagent region corresponds to the reaction coordinates ξ=−1.9 Å for Cl^- and ξ=−2.1 Å for Br^-, TS region with ξ=−0.35 Å for Cl^- and ξ=−0.5 Å for Br^-, and both products regions with ξ =1.0 Å. Only RDFs for Cl^- reaction at 450 K are shown here, as RDFs for Br^- are very similar and lead to the same conclusions. Reactions at 300 K were not fully converged as discussed in the previous section; hence, the RDFs calculated at 300 K might not represent the appropriate equilibrium distributions.

Figure 8 shows RDFs between solvent sites and the chloride ion. In the reagents, Cl^- is strongly solvated by $[BMIM]^+$. The sharp first peak at ~2.5 Å for the Cl–H2/H4 RDF suggests that hydrogen bonds are formed between Cl^- and the hydrogen atoms attached to the imidazole ring, in agreement with previous investigations.[51,6] The $[BMIM]^+$ methyl group has a positive charge density and, hence, coordinates the chloride in the reagents. Following reaction progress, Cl^- interacts with the *p*NBS methyl group and the negative charge is delocalized over the full reagent complex, as shown in Fig 10. The probability to find an imidazole ring-attached hydrogen in the first coordination shell around Cl^- decreases in the TS, suggesting that hydrogen bonds with Cl^- are broken in this reaction step. In the product region, the probability of finding a $[BMIM]^+$ methyl group coordinated to Cl^- decreases and it is approximately random (discounting the excluded volume), indicating that the interation of CH_3Cl with charged groups is small. This is expected from either chemical intuition, since CH_3Cl is a less polar molecule, or from the partial charges calculated for Cl^- and C0 (Fig. 10), which are close to 0 in the product region. On the other hand, the RDF between chloride and the terminal carbon from the $[BMIM]^+$ butyl group (C8, Fig. 8) shows that the environment around Cl becomes less polar and more hydrophobic with the reaction progress, again in line with calculated atomic charges. The solvation environment around the leaving group (*p*-nitrophenyl sulfonate) oxygen (OC) also changes. Figure 9 shows that the interaction of OC with positively charged groups in [BMIM] becomes more probable with reaction progress. Hydrogen bonds are also formed as indicated by the enhancement of the first peak in the RDF of the hydrogen atom attached to the imidazole ring (H1, see Fig. 1 for atom numbering). This is in line with the atomic charges calculated for this center (OC, Fig. 10) and with the development of a formal negative charge in the leaving

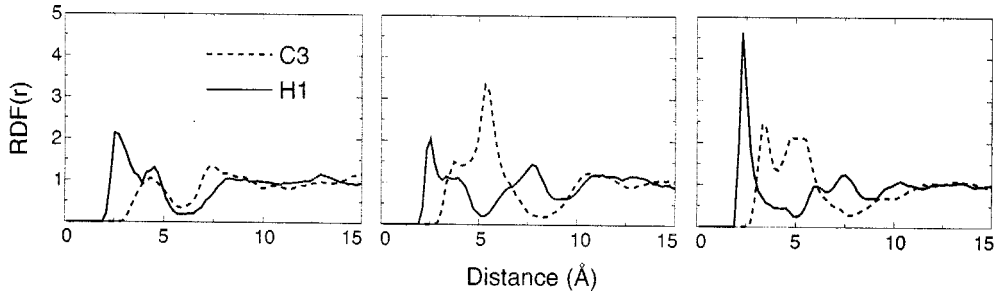

FIG. 9. Radial distribution functions at 450 K between the solute leaving group oxygen (OC) and different IL centers shown in the legend. See Fig. 1 for [BMIM] atom numbering. Left panel was obtained for the reagent region, middle panel for the TS region, and right panel for the product region.

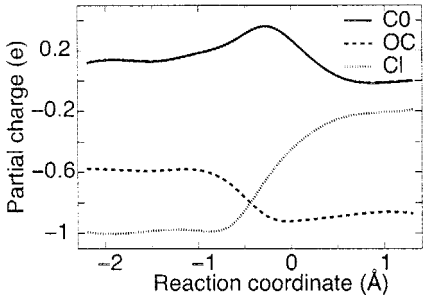

FIG. 10. Partial atomic charges calculated for the nucleophile Cl^-, *p*NBS methyl group (C0), and leaving group oxygen (OC) during reaction progress.

group. Hence, hydrogen bonds are formed between all three hydrogens attached to the imidazolium ring and either the nucleophile or the leaving group. This is in line with previous experimental studies.[51,6]

Inspection of the solute-solvent RDF for the Br^- reaction (data not shown) does not give any further structural indication on why this reaction is slower than the Cl^- reaction. In fact. the calculated barriers (see the previous section) and the measured reactivities for both halides in $[BMIM]PF_6$ are very similar (second order rate constants are 0.014 and 0.008 $M^{-1}\,s^{-1}$, respectively, for Cl^- and Br^- reactions with *p*NBS at 298 K),[6] and Lancaster cites a levelling effect by which the nucleophilicity of the two halides is almost the same in different ILs.[7]

Lancaster *et al.* proposed a reaction mechanism with a preequilibrium for nucleophile (Cl^-)-cation ($[BMIM]^+$) dissociation that would account for the differences observed in activation parameters measured for the halide substitution in ILs and in dicholoromethane.[7,6,5] This preequilibrium corresponds to desolvation of the nucleophile during its association with *p*NBS to form a reactant encounter complex. We have investigated this proposal by calculating potentials of mean force for reagent association from separations of 10 Å down to 3.5 Å between Cl^- and *p*NBS methyl carbon (data not shown). Over the larger distance, each reagent is in a different solvent cage and separated by at least one solvent species. Barriers for this process are smaller than 30 kJ/mol. Hence, a preequilibrium does not seem to be kinetically relevant and activation parameters should be unrelated to desolvation of the nucleophile for the reactions studied in this work. In fact, agreement between experimental and calculated barriers for the substitution reaction (Fig. 6) suggests that the chemical step only accounts for the kinetics.

IV. CONCLUSIONS

Computer simulations of halide substitution reactions toward methyl *p*-nitrobenzenesulfonate solvated by $[BMIM]PF_6$ were presented. A hybrid QM/MM potential containing a specific parametrized QM description of the reagents was used. Calculated reaction barriers are in reasonable agreement with experiment suggesting that the simulated model is a realistic one. Analysis of the microscopic solvation structure around reaction species revealed extensive hydrogen bonding between hydrogens attached to the imidazolium group of $[BMIM]PF_6$ and either the charged nucleophile or the leaving group.

Solvation by $[BMIM]PF_6$ in this substitution reaction correlates with charge density variation along the reaction coordinate. The IL behaves as an electrolyte solvent, and its role is comparable to polar molecular solvents such as water. In IL, decrease of the reaction velocity and increase of the reaction barrier, in comparison with a nonpolar solvent such as dichloromethane, are due to a better solvation of the reagent with a localized negative charge (Cl^- or Br^-) than solvation of the charge delocalized TS for the two reactions studied. This is, indeed, the classical Hughes–Ingold interpretation of solvent effects on the rates of nucleophilic substitution reactions.[8,9,49]

We are now calculating transmission coefficients for the same halide substitution reactions solvated by $[BMIM]PF_6$. These simulations will help us to determine the role of ILs on dynamical recrossings over the reaction barrier top and, consequentely, on reaction rates.

ACKNOWLEDGMENTS

The authors acknowledge financial support from FAPESP (via Project Nos. 2005/03995-7 and 2007/02371-5 to G.M.A.), CNPq and USP. Mark Kobrak (Brooklyn College, CUNY, USA) is also acknowledged for comments on an early version of this manuscript.

[1] J. Dupont, R. F. de Souza, and P. A. Z. Suarez, Chem. Rev. (Washington, D.C.) **102**, 3667 (2002).
[2] T. Welton, Coord. Chem. Rev. **248**, 2459 (2004).
[3] J. B. Harper and M. N. Kobrak, Mini-Rev. Org. Chem. **3**, 253 (2006).
[4] N. L. Lancaster, T. Welton, and G. B. Young, J. Chem. Soc., Perkin Trans. 2 **2001**, 2267.
[5] N. L. Lancaster, P. A. Salter, T. Welton, and G. B. Young, J. Org. Chem. **67**, 8855 (2002).
[6] N. L. Lancaster and T. Welton, J. Org. Chem. **69**, 5986 (2004).
[7] N. L. Lancaster, J. Chem. Res., Synop. **2005**, 413.
[8] E. D. Hughes and C. K. Ingold, J. Chem. Soc. **1935**, 244.
[9] E. D. Hughes and C. K. Ingold, Trans. Faraday Soc. **37**, 657 (1941).
[10] M. J. Kamlet, J. L. Addoud, and R. W. Taft, J. Am. Chem. Soc. **99**, 6027 (1977).
[11] C. Reichardt, *Solvents and Solvent Effects in Organic Chemistry*, 2nd ed. (VCH, Cambridge, 1998).
[12] C. J. Margulis, H. A. Stern, and B. J. Berne, J. Phys. Chem. B **106**, 12017 (2002).
[13] T. I. Morrow and E. J. Maginn, J. Phys. Chem. B **106**, 12807 (2002).
[14] J. de Andrade, E. S. Bes, and H. Stassen, J. Phys. Chem. B **106**, 13344 (2002).
[15] S. M. Urahata and M. C. C. Ribeiro, J. Chem. Phys. **120**, 1855 (2004).
[16] Y. Shim, J. Duan, M. Y. Choi, and H. J. Kim, J. Chem. Phys. **119**, 6411 (2003).
[17] C. G. Hanke and R. M. Lynden-Bell, J. Phys. Chem. B **107**, 10873 (2003).
[18] C. Hanke, A. Johansson, J. Harper, and R. Lynden-Bell, Chem. Phys. Lett. **374**, 8590 (2003).
[19] V. Znamenskiy and M. N. Kobrak, J. Phys. Chem. B **108**, 1072 (2004).
[20] Z. Hu and C. J. Margulis, Proc. Natl. Acad. Sci. U.S.A. **103**, 831 (2006).
[21] O. Acevedo, W. L. Jorgensen, and J. D. Evanseck, J. Chem. Theory Comput. **3**, 132 (2007).
[22] M. J. Field, P. A. Bash, and M. Karplus, J. Comput. Chem. **11**, 700 (1990).
[23] M. J. Field, M. Albe, C. Bret, F. P.-D. Martin, and A. Thomas, J. Comput. Chem. **21**, 1088 (2000).
[24] M. J. Field, J. Comput. Chem. **23**, 48 (2002).
[25] M. J. Frisch, G. W. Trucks, H. B. Schlegel, *et al.*, GAUSSIAN 98, revision

A.9, Gaussian Inc., Pittsburgh, PA, 1998.
[26] C. Lee, W. Yang, and R. Parr, Phys. Rev. B **37**, 785 (1988).
[27] A. D. Becke, J. Chem. Phys. **98**, 5648 (1993).
[28] R. Ditchfield, W. Hehre, and J. A. Pople, J. Chem. Phys. **54**, 724 (1971).
[29] E. Bright Wilson, Jr., J. C. Decius, and P. C. Cross, *Molecular Vibrations: The Theory of Infrared and Raman Vibrational Spectra*, 1st ed. (Dover, New York, 1980).
[30] T. Helgaker, P. Jørgensen, and J. Olsen, *Molecular Electronic-Structure Theory*, 1st ed. (Wiley, New York, 2000).
[31] R. Krishnan, J. Binkley, R. Seeger, and J. Pople, J. Chem. Phys. **72**, 650 (1980).
[32] M. J. Dewar, E. G. Zoebisch, H. F. Healy, and J. P. P. Stewart, J. Am. Chem. Soc. **107**, 3902 (1985).
[33] J. J. P. Stewart, J. Comput. Chem. **10**, 209 (1989).
[34] I. Rossi and D. G. Truhlar, Chem. Phys. Lett. **233**, 231 (1995).
[35] G. M. Arantes and M. Loos, Phys. Chem. Chem. Phys. **8**, 347 (2006).
[36] G. Menegon, K. Shimizu, J. Farah, L. Dias, and H. Chaimovich, Phys. Chem. Chem. Phys. **4**, 5933 (2002).
[37] D. Rinaldi, P. E. Hoggan, A. Cartier, K. Baka, G. Monard, M. Loos, A. Mokrane, V. Dillet, and V. Thery, GEOMOP, Nancy, France, 2001.
[38] W. L. Jorgensen, D. S. Maxwell, and J. Tirado-Rives, J. Am. Chem. Soc. **118**, 11225 (1996).
[39] T. I. Morrow and E. J. Maginn, J. Phys. Chem. B **107**, 9160 (2003).
[40] R. C. Rizzo, J. Tirado-Rives, and W. L. Jorgensen, J. Med. Chem. **44**, 145 (2001).
[41] J. Wang, W. Wang, P. A. Kollman, and D. A. Case, J. Mol. Graphics Modell. **25**, 247 (2006).
[42] B. Roux, Comput. Phys. Commun. **91**, 275 (1995).
[43] M. Allen and D. Tildesley, *Computer Simulation of Liquids*, 1st ed. (Oxford University Press, New York, 1987).
[44] F. P.-D. Martin, R. Dumas, and M. J. Field, J. Am. Chem. Soc. **122**, 7688 (2000).
[45] M. J. Field, *A Practical Introduction to the Simulation of Molecular Systems*, 1st ed. (Cambridge University Press, Cambridge, 1999).
[46] A. Thomas, D. Jourand, C. Bret, P. Amara, and M. J. Field, J. Am. Chem. Soc. **121**, 9693 (1999).
[47] S. M. Urahata and M. C. C. Ribeiro, J. Chem. Phys. **122**, 024511 (2005).
[48] E.-G. Kim and W. L. Mattice, J. Chem. Phys. **117**, 2389 (2002).
[49] S. S. Shaik, H. B. Schlegel, and S. Wolfe, *Theoretical Aspects of Physical Organic Chemistry: The S_N2 Mechanism*, 1st ed. (Wiley, New York, 1992).
[50] R. D. Guthrie and W. P. Jencks, Acc. Chem. Res. **22**, 343 (1989).
[51] A. G. Avent, P. A. Chaloner, M. P. Day, K. R. Seddon, and T. Welton, J. Chem. Soc. Dalton Trans. **1994**, 3405.